ICSO 2016

International Conference on Space Optics

Biarritz, France

18–21 October 2016

Edited by Bruno Cugny, Nikos Karafolas and Zoran Sodnik

A coronagraph for operational space weather predication

Kevin F. Middleton

esa icso proceedings cnes

International Conference on Space Optics — ICSO 2016, edited by Bruno Cugny, Nikos Karafolas, Zoran Sodnik, Proc. of SPIE Vol. 10562, 105620R · © 2016 ESA and CNES
CCC code: 0277-786X/17/$18 · doi: 10.1117/12.2297704

A CORONAGRAPH FOR OPERATIONAL SPACE WEATHER PREDICTION

Kevin F. Middleton,[1], Heiko Anwand,[5], Volker Bothmer,[5], Jackie A. Davies,[1], Klaus Ergenzinger,[2], Chris J. Eyles,[1], Jean-Philippe Halain,[3], Robert Hardie,[1], Marie-Laure Hellin,[3], Johannes Hinrichs,[5], Philipp Huke,[5], Niall Kennedy,[1], Volker Kirschner,[4], Piers Jiggens,[4], Christina McQuirk,[1], Bogdan Nicula,[6], Etienne Renotte,[3], Bryan M Shaugnessy,[1], Lars Stopfkuchen,[2], S. James Tappin,[1], Ian A. J. Tosh,[1], Nick R. Waltham,[1], Matthew J. West,[6]

[1]RAL Space, STFC Rutherford Appleton Laboratory, UK, [2]Airbus DS Space Systems, Germany, [3]CSL – Centre Spatial de Liège, Belgium, [4]European Space Research and Technology Centre (ESTEC), The Netherlands, [5]Institut für Astrophysik, University of Göttingen, Germany, [6]Royal Observatory of Belgium, Belgium

I. INTRODUCTION

Accurate prediction of the arrival of solar wind phenomena, in particular coronal mass ejections (CMEs), at Earth, and possibly elsewhere in the heliosphere, is becoming increasingly important given our ever-increasing reliance on technology. The potentially severe impact on human technological systems of such phenomena is termed space weather. A coronagraph is arguably the instrument that provides the earliest definitive evidence of CME eruption; from a vantage point on or near the Sun-Earth line, a coronagraph can provide near-definitive identification of an Earth-bound CME. Currently, prediction of CME arrival is critically dependent on ageing science coronagraphs whose design and operation were not optimized for space weather services. We describe the early stages of the conceptual design of SCOPE (the Solar Coronagraph for OPErations), optimized to support operational space weather services.

II. REQUIREMENTS

Current space weather services are critically reliant on images provided by a limited number of science coronagraphs onboard science missions, in particular the LASCO C2 and C3 instruments [1] on SOHO. The COR-1 and COR-2 coronagraphs on STEREO [2] also provide valuable supplementary information during certain orbital phases of the mission. To define the top-level requirements for the SCOPE instrument we asked members of the space weather forecasting community about the perceived benefits and limitations of current coronagraph data and what would be needed to optimize the operational service. The responses were translated into a set of requirements. Some requirements were specified with a threshold value (the minimum acceptable) and a goal (the ideal). All the thresholds should be met, with goals being achieved if they do not unduly drive cost, complexity or risk. Here we explore just a few of the top-level requirements, namely field of view (FOV), pixel scale, cadence and signal-to-noise ratio (SNR).

A coronagraph's FOV is usually expressed as the radial distance from the Sun's centre, calculated by making a plane-of-sky (POS) approximation. We define an outer FOV (the maximum extent of the image) and an inner FOV (the maximum distance at which the solar disc is still fully occulted). To predict Earth-arrival time with any degree of accuracy, CME imagery is required during that part of a CME's propagation when it has entered its so-called cruise phase, after which it is assumed to maintain a relatively constant speed. CMEs undergo their greatest acceleration in the lower corona, generally at less than a few R (solar radii) [3] [4], although they may also undergo further changes in speed throughout their propagation, due to energy exchange with the ambient solar wind (drag). The most critical region for obtaining images for forecasting is taken to be between some 5 and 22 R, which, on average, provides sufficient images of cruise phase to provide an accurate estimate of at least the initial CME speed; drag is included in some endeavors to model CME arrival time predictions. We set a threshold for the outer FOV limit of SCOPE of 22 R, and a goal outer FOV of 30 R – to capture more images of the cruise phase and to match LASCO C3's outer limit for compatibility with existing observations. The location of the inner FOV drives requirements on stray-light rejection and (in combination with the outer FOV) dynamic range. Observation of solar wind structures relies on the detection of sunlight that has been Thomson-scattered by electrons (the so-called K-corona, which includes both quasi-static components, like streamers, and more transient structures like CMEs). The Thomson-scattered signal must be extracted from other in-field signals that can be orders of magnitude greater (particularly that from the F-corona). This is illustrated by Fig. 1, which shows the K-corona (including the CME signal) and the much brighter background F+K corona against which any CME must be detected, both presented as a fraction of the mean solar brightness (MSB). The relatively low CME signal means that a high degree of suppression of signals from out-of-field sources, in particular stray-light from the Sun itself, is also required. Rejection of solar stray-light becomes more difficult as the inner FOV limit is decreased. The instrument must also be able to image the entire scene (including

background) without saturation, and this requires greater dynamic range as the inner FOV limit is decreased. Although scientifically interesting, there is no strong imperative (at least currently) to go much below 5 R for forecasting. We set a threshold inner FOV of 3 R (again giving compatibility with C3). We set ourselves a goal of 2.5 R in order to explore how far the instrument design can be pushed.

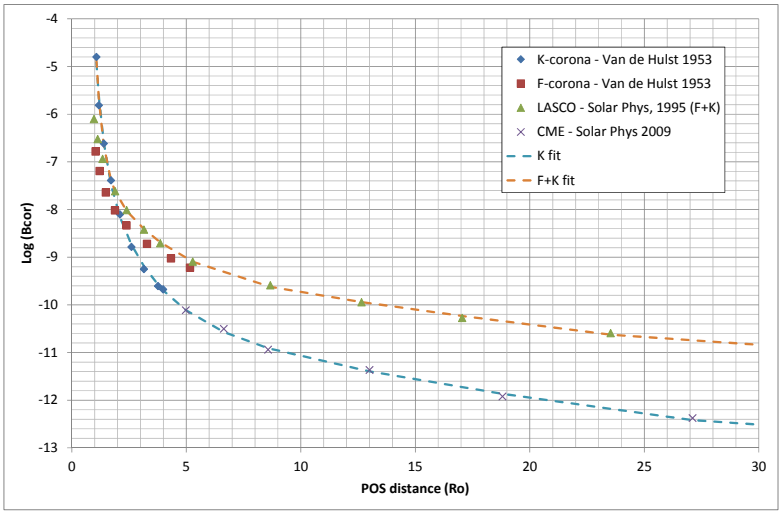

Fig. 1. Total coronal (F+K) brightness [1] [5] and K-corona brightness [6] as a fraction of the MSB (log scale)

CMEs have been observed that travel at speeds between 20 and 3,200 km/s [7] [8] with the average speed being around 500 km/s. Slower CMEs tend to have a smaller impact on the Earth and it is the fastest that, in general, produce the largest geomagnetic storms [9]. Table 1 shows the time that a CME would spend in the SCOPE threshold FOV, as well as the number of images of it that would be collected at 5 and 10 minutes image cadence, for a number of POS speeds. Aside from direct coronagraph observations, forecasters rely on supplementary tools and models when making CME arrival time predictions, such as the cone model [10], the CAT tool [11], CACTus [12], CORIMP [13], ARTEMIS [14], SEEDS [15], ENLIL [16] and drag-based models [17]. A minimum of around 5 images is desirable for forecasters to make a reasonable estimate of the CME speed. CACTus requires at least 7 images to make an accurate prediction. Forecasters generally agree that a 5 minute cadence is desirable but a 10 minute cadence is acceptable for most CME detections. For SCOPE we adopt a threshold cadence of 10 minutes and a goal of 5 minutes, allowing 7 images for all but the fastest of CMEs.

Table 1. POS CME speeds, the time spent in the SCOPE threshold FOV (3 – 22 R) and the number of images collected at 5 and 10 minute cadence. All values rounded to the nearest integer

CME POS speed (km/s)	Time in SCOPE threshold FOV (min)	No. images at 5 min cadence	No. images at 10 min cadence
300	734	147	73
500	440	88	44
1000	220	44	22
3500	63	13	6

While a smaller pixel scale (angular subtense per image pixel) allows the user to ascertain better the substructure within CMEs, for forecasting use of a 1024 × 1024 format over a 30 R FOV (consistent with C3's image format) is considered more than adequate. This corresponds to a pixel scale of 56 arcsec / pixel. We expect to have the option of binning the image and (rounding to the nearest arc minute) we adopt a plate scale of 2 arcmin / pixel as a threshold, corresponding to 512 x 512 pixels over a 30 R FOV, and 1 arcmin / pixel as a goal, corresponding to 1024 x 1024. In this case, we expect to meet both goal and threshold requirements without difficulty by appropriate binning.

To determine the minimum acceptable SNR we adopted two parallel approaches. The first was to analyse existing C3 images to estimate the actual SNR, whereas the second was to generate artificial images and then add noise to see how CME detection was affected. The SNR is defined as the SNR per pixel, where the signal comprises the detected photo-electrons from the CME and the noise includes sources inherent to the instrument (such as detector read-noise and stray-light noise) and external sources such as shot-noise on the background K+F corona. Fig. 2 shows a typical result from the first method. Starting from LASCO level 0.5 data, images were back-converted from DN (data number) to photo-electrons by subtracting any bias and then applying an

assumed system gain of 17.5 electrons / DN [1]. To detect CMEs, the background (mainly F-corona, stable stray-light and stable K-corona) must be subtracted. In our case this was estimated by taking the lower quartile of the values in each pixel (normalized to the exposure time) from a series of images spanning one day. After background subtraction, the SNR was calculated assuming the resulting signal to be shot-noise limited. Typical CMEs were found to have an SNR between 2 and 4 at the edge of the FOV.

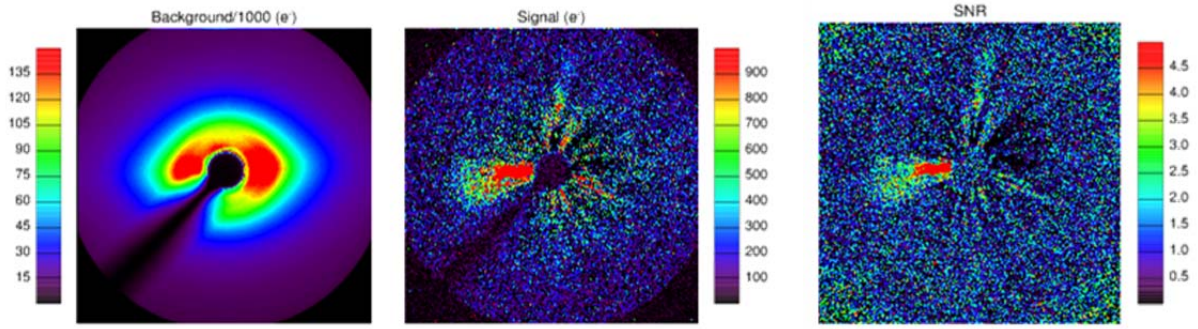

Fig. 2. Images of background (left), CME signal (centre), SNR (right).

For the second method, a series of simulated images were constructed using LASCO level 0.5 data as a basis for realistic header information. A coronal background was calculated using experimentally derived formulae [18] [19] and the image of a CME-fluxtube was generated with the ray tracing code of the SolarSoft routine GCS [20]. The images were generated so that the CME moves with constant velocity. A scaling factor for CME brightness relative to the corona was applied to the CME image, which was then added to the coronal image. The whole image was then scaled to give the number of photo-electrons required for the intended SNR level at the edge of the FOV and shot-noise added. Finally the image was scaled to the DN of a real image and corrected to account for exposure time and offsets from real observations. Fig. 3 shows simulated CMEs with an SNR of 1, 4 and 10. In all cases the leading edge of the CME can be discerned, suggesting that an SNR as low as 1 is sufficient for visual detection. The simulated images were passed through CACTus [12], an algorithm for the automatic detection of CMEs in coronagraph imagery. CACTus consistently showed no clear CME detections at SNR values lower than 4. At this value, the (overall) absolute noise level in the simulated images was similar to the level in real images. Below this value, false detections start to appear at all times and position angles, with CATUS appearing to misidentify noise as CMEs. For SCOPE, the threshold SNR was set to 2 and the goal to 4. The logic for this was that an SNR of 4 allows automated detection of CMEs on the ground using CACTus whereas and SNR of 2 still allows their robust detection by a human observer.

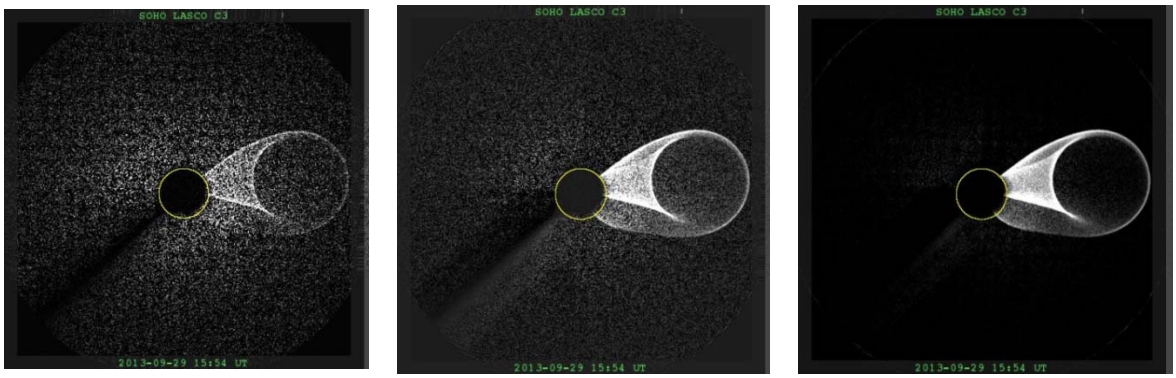

Fig. 3. Screenshots for the SolarSoft routine CAT, showing difference images of simulated CMEs with SNR of 1 (left), 4 (centre) and 10 (right)

Table 2 gives a summary of the resulting top-level requirements for SCOPE.

Table 2. Summary of top-level requirements for SCOPE

Parameter	**Threshold value**	**Goal value**
FOV	3 – 22 R	2.5 – 30 R
Min SNR per pixel	2	4
Plate scale	2 arc min / pixel	1 arc min / pixel
Image array size	512 x 512	1024 x 1024
Cadence	One image every 10 minutes	One image every 5 minutes

III. BASELINE DESIGN

Fig. 4 shows the design concept for SCOPE. The corona is imaged directly onto the detector by a single objective lens system, resulting in a more compact optical design [21] than traditional coronagraphs [1]. An external occulter (EO) that blocks light from the solar disc out to the inner FOV limit is placed in front of the lens. A baffle tube blocks stray-light scattered off instrument surfaces and sources outside the FOV. An internal occulter (IO), positioned just in front of the detector, can be used to block diffracted stray-light that makes it past the EO and is focused near the detector (whether this is in fact necessary, or whether an EO only will suffice, is currently under investigation).

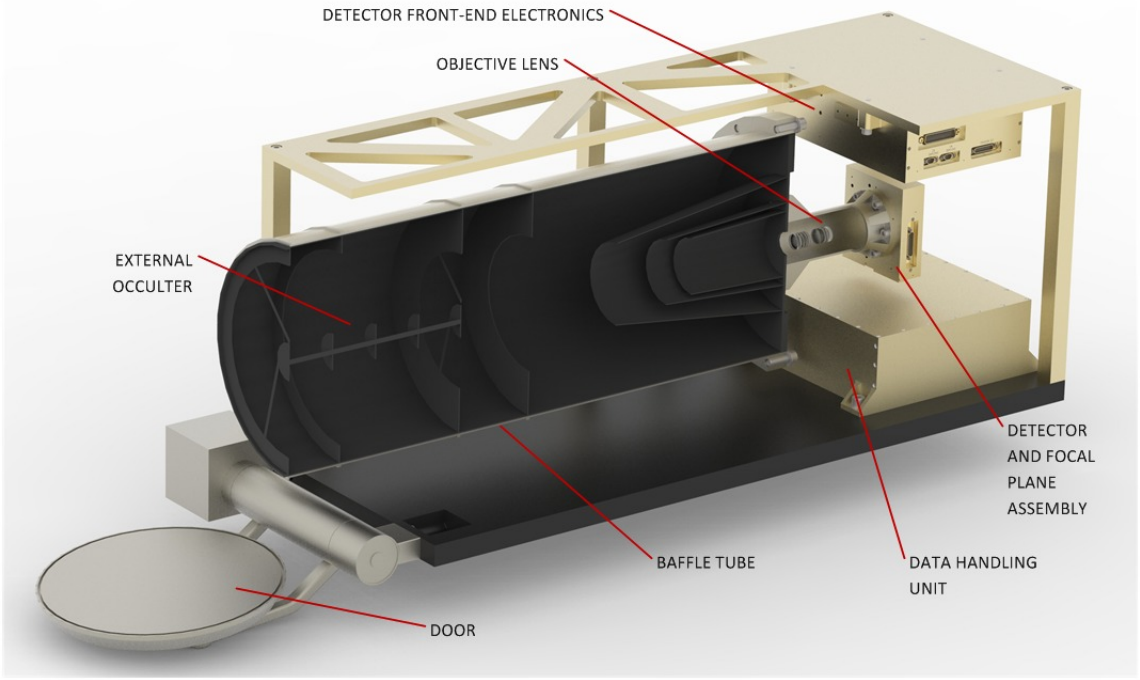

Fig. 4. Mechanical layout of SCOPE.
(Not shown: mounting of baffle tube to structure, harnesses, shutter, internal occulter)

To develop the system design, a radiometric model was built in Microsoft Excel to allow the prediction of signal and noise levels. This allowed a number of different instrument configurations to be explored, varying parameters such as entrance pupil (EP) diameter, distance from EO to EP, exposure time, number of exposures and detector format. The philosophy was to design the instrument to be shot-noise limited after subtraction of the coronal background. After comparing a number of different design configurations we arrived at a baseline, summarized in Table 3. For computing SNR and fraction of detector full-well capacity, the model uses the coronal and CME brightness values of Fig. 1.

Table 3. Summary of the SCOPE baseline design

Parameter	**Values**	**Units**	**Notes**
Aperture diameter	25	mm	
Physical detector format	2048 x 2048	pixels	Bin to 1024 x 1024 or 512 x 512
Pixel size (physical detector pixel)	15	µm	Bin to 30 µm or 60 µm
Overall length	710	mm	Front of baffle tube to detector
Exposure time	3.2	s	
No. exposures	3	-	3 exposures are combined into one image
Effective total time to take one image	11.6	s	Total for 3 exposures, including read-out time
Fraction of used full-well capacity	38%	-	Per exposure (see Fig. 5)
Limiting R for vignetting	5.6	R	FOV at which vignetting no longer degrades image quality
SNR at 22 R	9.1	-	SNR per pixel for 1 image (3 combined exposures)
SNR at 30 R	4.5	-	SNR per pixel for 1 image (3 combined exposures)

Fig. 5 shows the output of the radiometric model for the baseline design. The upper plots show the SNR and detector full well usage (top left), and a breakdown of noise sources (top right). The lower plots show the specification for stray-light. This is derived by assuming that the contribution from stray-light at any point in the image should be less than 20% of the coronal brightness. This can be expressed as an equivalent stray-light brightness relative to the MSB (bottom left) and also as a quantity that we define as solar source transmittance (SST – bottom right), taken as the ratio of the stray-light irradiance at the focal plane to the solar irradiance at the entrance to the baffle tube. The SST is a convenient quantity when analyzing performance.

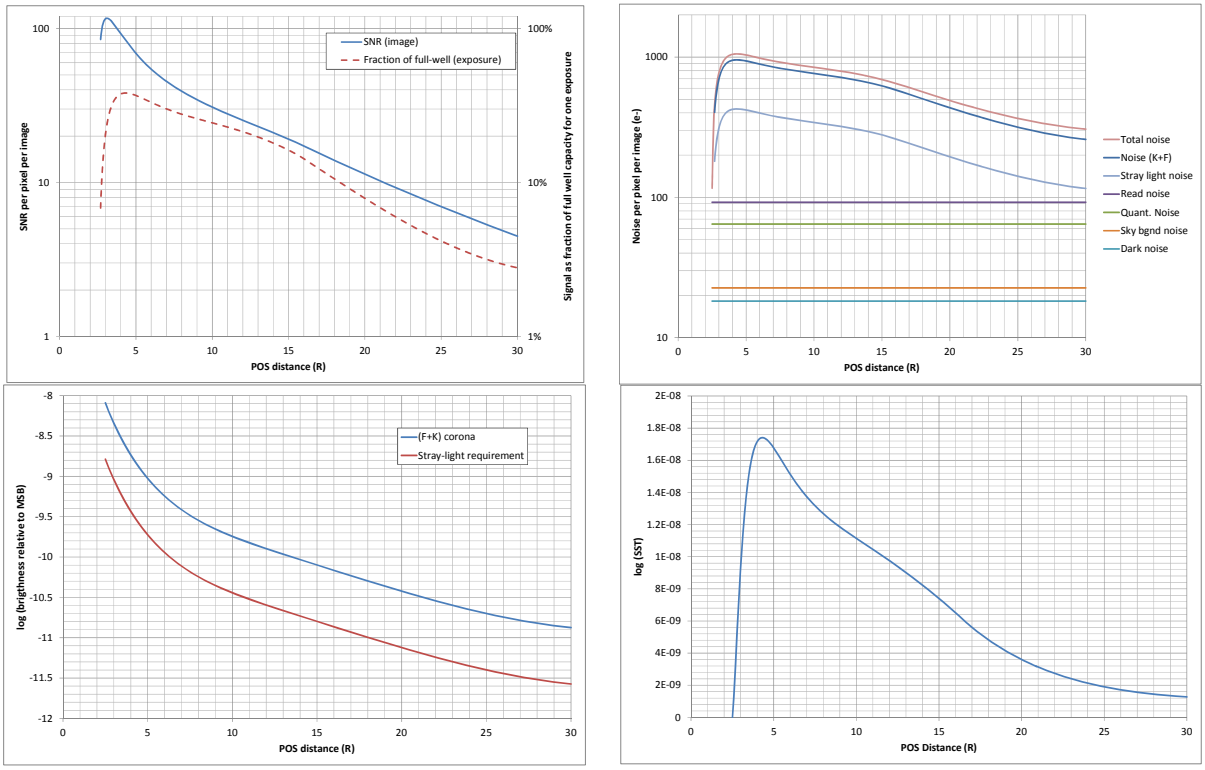

Fig. 5. Outputs from the radiometric model for a design meeting the goal requirements from Table 2: SNR and fraction of full well capacity used (top left); breakdown of noise sources (top right); stray-light as fraction of MSB (bottom left); stray-light as SST (bottom right)

An image is constructed by combining a number (in this case 3) of exposures. The total time to collect the image is constrained to be less than the time taken for the fastest CMEs to cross one pixel (although this is not a hard limit on performance). Combining multiple exposures allows for removal of image contamination 'snow', which occurs due to solar energetic particles (SEPs), by comparing successive exposures – a process known as 'cosmic ray scrubbing' (SEPs are often associated with CMEs). One of the key design decisions is the choice of sensor technology between CCD and CMOS. A full trade study is underway but the results are tending towards the use of CCD, primarily due to its larger full-well capacity and the availability of sensors with pixel sizes best matched to the optical design requirements (a relatively large pixel, 15 µm or greater, helps make the optical design easier). The baseline is to use a 2048 x 2048, 15 µm pixel sensor (for example, the e2v CCD230) and bin off-chip to 1024 x 1024 or 512 x 512. Although a CCD allows on-chip binning without the introduction of additional read-noise, binning off-chip gives additional flexibility when performing the cosmic ray scrubbing. We do not envisage the use of a shutter to control exposures and instead propose using techniques developed for STEREO/HI [22] to remove artefacts due to smearing of the image during CCD line transfer. This correction can degrade the SNR by up to a factor 2 (in the very worst case, if a frame transfer CCD is not used) but we allow for this by building sufficient margin into our SNR (Table 3) so that the threshold is met in all cases.

A key aspect of the performance of a coronagraph is the stray-light rejection. This requires careful control of light diffracted at the occulter baffles to prevent it reaching the sensor. Fig. 6 shows the provisional objective lens design. This uses a radiation stabilized glass as its first element and is designed for a beam clearance out to 40 R, reducing stray-light reflected from lens edges and mounts. The EP is placed in front of the lens system to aid stray-light control. Fig. 6 also shows an early iteration of the baffle layout inside the baffle tube. A series of 5 occulter discs (D1 – D5) is used to block light from the solar disc, with each occulter optimized to block, as efficiently as possible, diffracted light from the previous one following the method of Halain [23]. Further vanes

(V1 – V5) and conical baffles (C1 – C5) block all direct scatter paths for incoming solar radiation to the EP and minimise as far as possible double bounce paths (mainly between the back face of the baffle tube and V1/V3/D1). Further optimization is ongoing (for example, exploring the option of making D1-D5 conical [24] to form a cavity, reducing back-scatter into the EP).

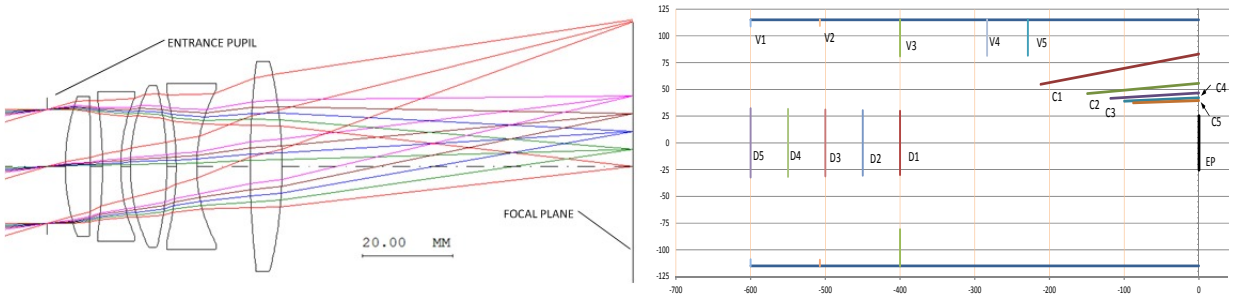

Fig. 6. Objective lens design (left); preliminary baffle layout (right)

The most critical aspect of assessing the stray-light rejection is in computing the diffracted solar light that makes it past the series of occulters. To assess this, one must solve the Fresnel diffraction integral. We used two approaches: the first was to write in-house code; the second was to use GLAD (Applied Optics Research). Fig. 7 shows the results from GLAD. In this case the stray-light attenuation is computed between the entrance to the baffle tube and the entrance pupil, and is taken as being the ratio of the irradiance in the two planes when illuminated with a point source at infinity. The results show broad agreement with simulations from previous coronagraphs [21] [24] [25] and there is also agreement between GLAD and our in-house code. Work is ongoing to assess the end-to-end stay-light performance to give predicted stray-light at the focal plane including the Sun as an extended source.

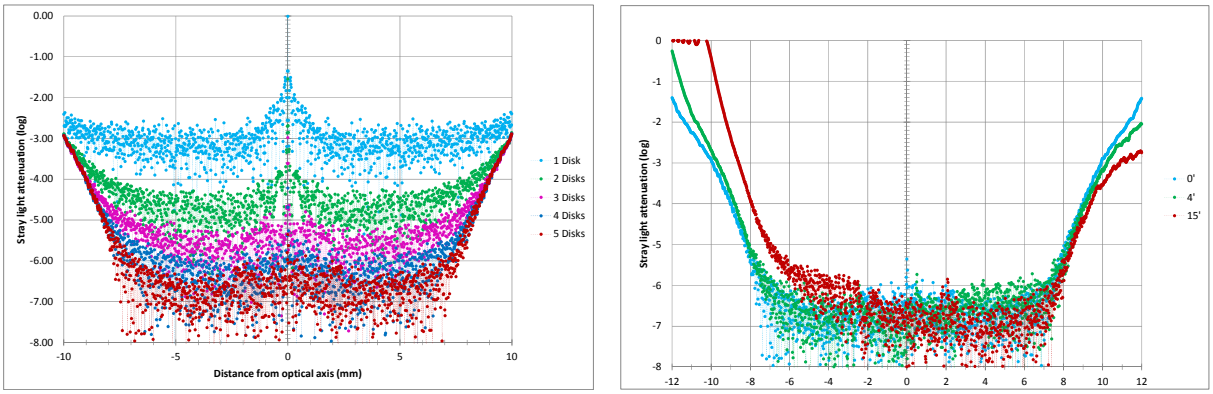

Fig. 7. Variation in stray-light attenuation with an increasing number of occulter discs (all discs at 50 mm spacing - left) and with off-axis source position (5 discs - right).

Fig. 8 shows the electronics architecture. The detector FEE (front-end electronics), housed in a separate enclosure, passes image data to an instrument DHU (data handling unit). The DHU provides local image storage and some basic image processing, including cosmic ray scrubbing. The possibility of also performing some on-board processing to identify CMEs is currently under investigation. The DHU also manages thermal control of the instrument and controls any mechanisms. Mechanism options are currently being assessed but the most likely configuration is a single-shot door at the entrance to the baffles (to prevent contamination before the start of operations) and a multiple actuation shutter, positioned in front of the objective lens to protect against accidental direct solar viewing (but not to control exposures – this is not deemed necessary, as previously explained). The DHU is currently based on a reference design that will be tailored to the specific mission requirements later in the study. It is conceived as an integrated unit comprising separate processing and power modules. The design uses space-qualified components with high TRL. The processor comprises a LEON2-FT software processor implemented in a system-on-chip radiation hardened ASIC. The FEE, also at high TRL, is based on an ITAR-free version of the SDO AIA/HMI and GOES-R SUVI camera electronics boxes currently under development for the WSO mission [26]. The core functionality of the FEE is provided by single PCB design using a single FPGA. This reduces the number of lower grade components, improves system reliability and reduces the power requirement. The video signals from the CCD are digitised using CDS/ADC ASICs [27]. These provide the correlated double sampling (CDS) and analogue-to-digital conversion (ADC) required to sample and digitise the video signals from the CCD's readout amplifiers. The ASICs (one per CCD output port)

run in parallel and provide 16-bit digitisation. The digitised data are multiplexed within the FPGA and transmitted to the DHU via a SpaceWire interface, implemented using a SpaceWire core in the FPGA. This SpaceWire interface also provides the control interface to the FEE allowing the CCD bias voltages to be programmed and telemetry read back to the DHU. It also provides an interface to the internal programmable waveform generator and sequencer (WGS) and the CCD clock driver circuitry. The WGS defines the camera's CCD and video signal processing electronics timing signals with a typical resolution of 50 ns. CCD clock drivers translate the WGS logic-level outputs into high-current drive waveforms of appropriate amplitude and shape to drive the CCD's capacitive electrodes and gates. A reliability assessment of the DHU and FEE is currently underway, from which parts requirements and a redundancy scheme (if any) will flow.

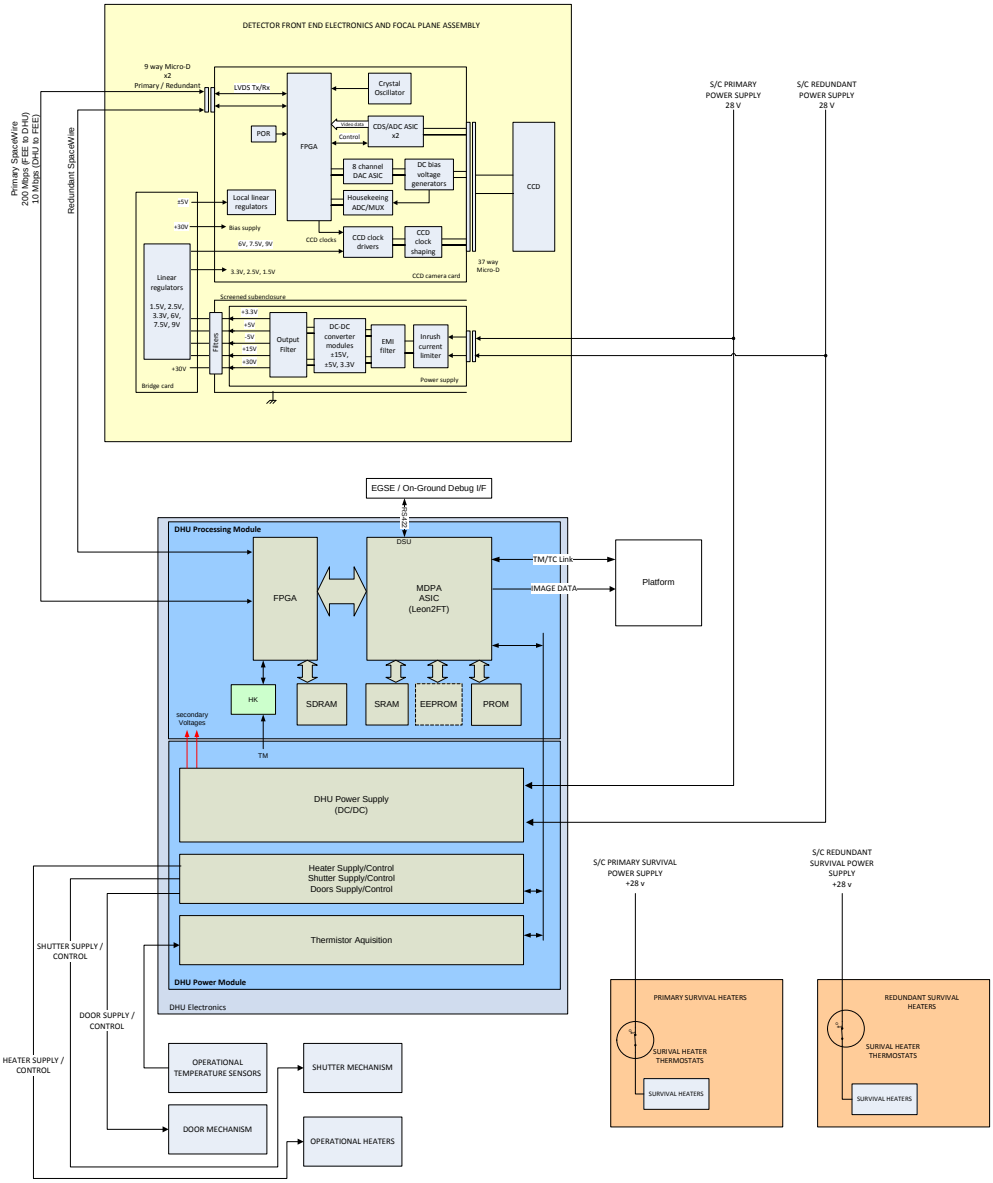

Fig. 8. SCOPE electrical architecture

IV. FURTHER WORK

The conceptual design will be further developed over the coming months, after which we plan to construct an optics breadboard (OBB). The goal of the breadboarding will be to characterize and confirm the stray-light rejection of the optical design. This is seen as the major risk area and successful characterization will allow progress to detailed design with a good level of confidence in the design. All other areas of the design are expected to be at sufficiently high TRL to allow detailed design to start once the conceptual design is finalized.

V. PROJECT TEAM

Table 4 shows the SCOPE consortium and lists their responsibilities during this phase of work.

Table 4. Consortium responsibilities

Institute	Responsibility
STFC RAL Space (lead)	User requirements analysis Conceptual design of flight instrument (optics, structure, thermal, electronics architecture, FEE and focal plane, mechanisms) Stray-light and baffle design
Airbus DS Space Systems	DHU hardware, DHU software (firmware and system), DHU power supply Assessment of mission and orbital environment
Centre Spatial de Liège	Stray-light tests on the optics breadboard
Royal Observatory of Belgium	DHU image processing software Support for user requirements analysis
University of Göttingen	Design and construction of the optics breadboard Support for user requirements analysis

ACKNOWLEDGEMENTS

This work was performed under the ESA Contract No. 4000116072/15/NL/LF as part of ESA's General Support Technology Programme (GSTP).

REFERENCES

[1] G. E. Brueckner, *et al*, "The Large Angle Spectroscopic Coronagraph (LASCO)", *Solar Phys,* 162, 357 – 402, 1995
[2] R.A. Howard, *et al*, "Sun Earth Connection Coronal and Heliospheric Investigation (SECCHI)", *Space Sci Rev* 136, 67–115, 2008
[3] St. Cyr, O.C., J.T. Burkepile, A.J. Hundhausen, and A.R. Lecinski, *JGR,* 104, A6, 12493, 1999
[4] Zhang, B., & Mészáros, P., *ApJ*, 559, 110, 2001
[5] van de Hulst, H. C. "The Chromosphere and Corona", in *The Sun* (G.P. Kuiper, ed), p. 207, Univ, of Chicago Press, 1953
[6] C.J. Eyles, *et al*, "The Heliospheric Imagers Onboard the STEREO Mission", *Solar Phys*, 254: 387–445, 2009
[7] D. F Webb, T. A Howard, "Coronal Mass Ejections: Observations", *Living Rev. Solar Phys.*, 9, 3, 2012
[8] V.G. Fainshtein, Yu. S. Zagaynova, "The beginning of halo CMEs", *Solar and Stellar Astrophysics*, arXiv:1208.5890, 2012
[9] A Kilcik *et al*, "Maximum Coronal Mass Ejection Speed As An Indicator Of Solar And Geomagnetic Activities", *ApJ*, 727:44, 2011
[10] Zhao, X. P., S. P. Plunkett, and W. Liu, "Determination of geometrical and kinematical properties of halo coronal mass ejections using the cone model", *J. Geophys. Res*., 107 (A8), 122, 2002
[11] G. Millward, D. Biesecker, V. Pizzo, and C. A. de Koning, "An operational software tool for the analysis of coronagraph images: Determining CME parameters for input into the WSA-Enlil heliospheric model", *Space Weather*, Vol. 11, 57–68, 2013
[12] E. Robbrecht and D. Berghmans, "Automated recognition of coronal mass ejections (CMEs) in near-real-time data", *A&A,* 425, 2004
[13] H. Morgan, J. P. Byrne and S. R. Habbal, "Automatically Detecting And Tracking Coronal Mass Ejections. I. Separation Of Dynamic And Quiescent Components In Coronagraph Images", *ApJ*, 752:144 (14pp), 2012
[14] Boursier, Y., Lamy, P., Llebaria, A., Goudail, F. and Robelus, S., "The ARTEMIS catalog of LASCO coronal mass ejections. Automatic recognition of transient events and Marseille inventory from synoptic maps", *Solar Phys.*, 257, 125–147, 2009
[15] Olmedo, O., Zhang, J., Wechsler, H. *et al*., "Automatic Detection and Tracking of Coronal Mass Ejections in Coronagraph Time Series" *Solar Phys*., 248: 485, 2008
[16] Odstrcil, D., and V. J. Pizzo, "Three-dimensional propagation of CMEs in a structured solar wind flow", *J. Geophys. Res*., 104, 483, 1999a.
[17] Vršnak, B.; Žic, T., "Transit times of interplanetary coronal mass ejections and the solar wind speed", *Astronomy and Astrophysics*, Volume 472, Issue 3, pp.937-943, 2007
[18] Baumbach, S.: "Strahlung, Ergiebigkeit und Elektronendichte der Sonnenkorona", *Astronomische Nachrichten,* 263, 121, 1937
[19] November, L. J., Koutchmy, S., "White-Light Coronal Dark Threads and Density Fine Structure", *ApJ,* 466, p. 512, 1996
[20] Thernisien, A.: Implementation of the Graduated Cylindrical Shell Model for the Three-Dimensional Reconstruction of Coronal Mass Ejections, *The Astrophysical Journal Supplement Series,* 194:33 (6pp), 2011 June
[21] Q. Gong, D. Socker, "Theoretical study of the occulted solar coronagraph" *Proc. SPIE* 5526, 208 – 219, 2004
[22] C.J. Eyles, et al, "The Heliospheric Imagers Onboard the STEREO Mission", *Solar Phys*, 254: 387–445, 2009
[23] J.-P. Halain, "Diffractive straylight rejection system for wide field imagers. Design, performance and application to the STEREO solar space mission", *PhD Thesis,* University of Liege, p32, 2012
[24] M Bout *et al*, "Experimental Study of External Occulters for the Large Angle and Spectrometric Coronagraph 2: LASCO-C2", *,Applied Optics*, Vol. 39, No. 22, 2000
[25] Thernisien A , "Experimental and Numerical Optimization of a Coronagraph External Occulter. Application to SECCHI-COR2 and GOES-R SCOR", *Solar Physics and Space Weather Instrumentation*, Proc SPIE OEI133, 2005
[26] M. Salter, M. Clapp, J. King, T. Morse, I. Mihalcea, N. Waltham, C. Hayes-Thakore, "Development of low-noise CCD drive electronics for the World Space Observatory Ultraviolet Spectrograph subsystem", *Proc. SPIE 9915*, 2016
[27] N. Waltham, Q. Morrissey, M. Clapp, S. Bell, L. Jones, M. Torbet, "The Design And Development Of Low- And High-Voltage Asics For Space-Borne Ccd Cameras", ICSO 2016, in press